The Structure of Bioactive Silicate Glasses: New Insight from Molecular Dynamics Simulations

Antonio Tilocca,*,† Alastair N. Cormack,†,‡ and Nora H. de Leeuw†,§

Department of Chemistry, University College London, United Kingdom, New York State College of Ceramics, Alfred University, Alfred, New York 14802, and School of Crystallography, Birkbeck College London, United Kingdom

Received July 13, 2006. Revised Manuscript Received September 20, 2006

The structural properties of three compositions of phosphosilicate glasses are investigated by means of molecular dynamics computer simulations using a new potential model incorporating polarization effects. Structural features of the three compositions are compared in order to highlight the effect of the composition on the different known bioactivities of these materials. Changes in the coordination environment, network connectivity, and ion aggregation with the silica content are discussed, as they enable us to draw a microscopic model of the glasses, which supports the interpretation of experimental data and provides new insight into the special physicochemical behavior of these materials. The transition from highly bioactive to bioinactive compositions is characterized by a marked increase in the connectivity of the silicate network and by an increasing fraction of phosphate groups involved in P−O−Si cross-links. Our analysis also highlights a possible correlation between the loss of bioactivity and a significant aggregation between Ca^{2+} and PO_4^{3-} ions, which leads to calcium-phosphate-rich regions for a bioinactive composition containing 65% SiO_2.

1. Introduction

Surface-active silicate glasses have been widely used in medical applications since their discovery in the early 1970s by Hench and co-workers[1−3] at the University of Florida. Unlike inert biomaterials, bioglasses show a strong active response after they are implanted in the human body or put in contact with a physiological medium. A series of chemical transformations occurs after implantation, which leads to the growth of a layer of crystalline hydroxy-carbonate apatite (HCA) on their surface; this layer then interacts with and incorporates biomolecules such as collagen, whereas further cellular steps lead to a strong and stable chemical bond between the glass and human hard (bone) and, in some cases, soft (muscle) tissues.[1] The bioactivity of these materials is routinely measured as the rate of HCA formation in vitro,[4−6] or of bone formation in vivo;[7,8] this rate varies considerably with the glass composition: for instance, the 45S5 composition, including 45% silica, crystallizes HCA on its surface within 2 h and binds to both soft and hard tissue.[1] Compositions incorporating between 53 and 58% of SiO_2 are less active, with HCA formation in 2−3 days, and they bond only to bone, whereas compositions of above 60% SiO_2 do not form crystalline HCA and are considered to be bioinactive. The reaction steps leading to the HCA formation have been roughly identified:[1] (a) initial leaching of Na^+ ions, which are replaced by H^+ from solution; (b) breaking of Si−O−Si bonds and release of soluble silica to the solution; (c) the surface silanol groups formed in both previous steps condense to form a silica-rich layer on the surface; (d) calcium and phosphate ions are released through this surface layer and incorporate other Ca^{2+} and PO_4^{3-} from solution to form an amorphous calcium phosphate phase; (e) the latter amorphous film incorporates additional carbonate ions from solution and crystallizes to HCA. By altering the glass composition, one can in principle tune the rate of HCA formation and the glass physical properties for a specific application; a more rational control of the bioactivity, however, could be achieved by establishing the microscopic, structural basis of the bioactive behavior and its relation with the composition. Any progress in this direction requires first a detailed description of the bulk structure of different compositions, possibly spanning a wide bioactivity range. This fundamental approach has been somewhat hindered by the intrinsic difficulty of applying standard solid-state experimental techniques to investigate the bulk structure of amorphous materials; however, thanks to techniques such as nuclear magnetic resonance (NMR),[9−11] Raman vibrational

* Corresponding author. E-mail: a.tilocca@ucl.ac.uk.
† University College London.
‡ Alfred University.
§ Birkbeck College London.

(1) *An Introduction to Bioceramics*; Hench, L. L., Wilson, J. Eds, World Scientific: Singapore, 1993.
(2) Hench, L. L. *Science* **1980**, *208*, 826.
(3) Hench, L. L.; Wilson, J. *Science* **1984**, *226*, 630.
(4) Martinez, A.; Izquierdo-Barba, I.; Vallet-Regi, M. *Chem. Mater.* **2000**, *12*, 3080.
(5) Oliveira, J. M.; Correia, R. N.; Fernandes, M. H. *Biomaterials* **2002**, *23*, 371.
(6) Cerruti, M.; Bianchi, C. L.; Bonino, F.; Damin, A.; Perardi, A.; Morterra, C. *J. Phys. Chem. B* **2005**, *109*, 14496.
(7) Vogel, M.; Voigt, C.; Gross, U. M.; Muller-Mai, C. M. *Biomaterials* **2001**, *22*, 357.
(8) Fujibayashi, S.; Neo, M.; Kim, H. M.; Kokubo, T.; Nakamura, T. *Biomaterials* **2003**, *24*, 1349.
(9) Lockyer, M. W. G.; Holland, D.; Dupree, R. *J. Non-Cryst. Solids* **1995**, *188*, 207.
(10) Clayden, N. J.; Pernice, P.; Aronne, A. *J. Non-Cryst. Solids* **2005**, *351*, 195.

10.1021/cm061631g CCC: $37.00
Published on Web 12/07/2006

spectroscopy,[5,12] and neutron diffraction,[13] some general ideas have started to emerge. The partial dissolution of the glass network involves the release of both network-modifier (i.e., Na and Ca) and network-former (Si and P) ions to the solution; because this process requires breaking chemical bonds (for Si and P) or overcoming electrostatic and dispersion forces (for Na and Ca), it is strongly affected by the local microenvironment of each species. Therefore, structural descriptors of the coordination environment, for both network formers and modifiers, are especially useful as predictive tools for the bioactivity. For network formers, the bonding environment can be characterized by the fraction of bridging oxygens (BO) in each SiO_4 and PO_4 polyhedron,[14,15] and the Q^n distributions, where Q^n ($n = 0-4$) is a Si or P ion bonded to n BOs.[9,11, 16,17] Because a BO connects two adjacent polyhedra, these factors determine the overall network connectivity (NC) of the glass: in general, a low NC, denoting a fragmented phosphosilicate network, will favor release of soluble silica and phosphate fragments to the solution. Indeed, NMR and Raman data show that silicon is predominantly Q^2 in highly bioactive compositions,[9,11,12] whereas Q^3 is the dominant Si species in compositions with lower bioactivity.[11,12] Previous predictive models[14,16,17] identified a range of NC $\approx 2-3$ for bioactive compositions; however, their success relies on specific assumptions on the coordination of silicon and (especially) phosphorus, whose actual role in the silicate network is rather controversial and needs further investigations. The inclusion of phosphorus, although not a prerequisite for bioactivity, leads to a higher rate of HCA formation:[19] PO_4 groups are predominantly isolated in Hench's silicate glasses[9-11] and are easily released in this form, enhancing the rate of formation of calcium phosphate film in stage (d). Indeed, the presence of polyphosphate chains turns out to inhibit bioactivity in these materials.[20] On the other hand, a fraction of P ions could be incorporated in the silicate network,[12] and the balance between free (isolated) and bound (incorporated in the glass network) phosphate could have important effects on the Si release rate.[19]

Much less structural information is available on the coordination environment of network modifier cations; the "repolymerizing" effect of phosphates on the silicate network, whereby they remove Na and Ca cations from the silicates and thus reduce the number of nonbridging oxygens (NBO) linked to Si,[9,18] seems to involve a preference of modifier cations for the phosphate groups. Differences in the structural arrangement and stability of Na and Ca coordination sites are crucial for the migration mechanism of these ions,[21,22] which in turn determine their dissolution rate. Moreover, the way in which cations are arranged around silicate and phosphate fragments affects the energetics and rates of breaking off and releasing these fragments into solution.

Further investigation of these key structural factors and issues can be greatly improved with the atomistic resolution of modern computational techniques, which could also unveil other relevant effects. Despite a significant number of molecular dynamics (MD) simulations investigating the properties of simple silicate and phosphate glasses,[23-31] not many computational studies of multicomponent phosphosilicate glasses have appeared so far, probably because of the lack of suitable potential models capable of incorporating the complex interactions and effects present in these materials. The parameter-free, unbiased approach of ab initio molecular dynamics[32] provides a powerful alternative, which has been applied recently to investigate structural and electronic effects in silicate glasses.[33-35] However, the limited space and time scales that can be afforded by ab initio approaches, even with state-of-the-art computational resources, do not allow us to explore structural features beyond local order, such as the network connectivity, that influence the bioactivity. When our interest is focused on these features, as in the present work, classical MD simulations still represent the best choice, provided that a reliable force field is available. We have recently developed a shell-model interatomic potential for silicate glasses, including Na and Ca network modifiers,[37] which has been shown to provide a reliable representation of structural and dynamical properties of sodium and soda-lime silicate glasses. In this paper, we perform MD simulations using this new potential (extended to include the interaction with phosphate groups) to provide accurate structural information on three different compositions of phosphosilicate glasses, with 45-55-65% SiO_2 (BG45, BG55, and BG65, respectively, in the following). These compositions have been selected in order to cover a wide bioactivity range, from highly active (BG45) to

(11) Elgayar, I.; Aliev, A. E.; Boccaccini, A. R.; Hill, R. G. *J. Non-Cryst. Solids* **2005**, *351*, 173.
(12) Lin, C. C.; Huang, L. C.; Shen, P. *J. Non-Cryst. Solids* **2005**, *351*, 3195.
(13) Skipper, L. J.; Sowrey, F. E.; Pickup, D. M.; Drake, K. O.; Smith, M. E.; Saravanapavan, P.; Hench, L. L.; Newport, R. J. *J. Mater. Chem.* **2005**, *15*, 2369.
(14) Strnad, Z. *Biomaterials* **1992**, *13*, 317.
(15) Borrajo, J. P.; Liste, S.; Serra, J.; Gonzalez, P.; Chiussi, S.; Leon, B.; Perez-Amor, M. *Key Eng. Mater.* **2005**, *17*, 465.
(16) Hill, R. G. *J. Mater. Sci. Lett.* **1996**, *15*, 112.
(17) Wallace, K. E.; Hill, R. G.; Pembroke, J. T.; Brown, C. J.; Hatton, P. V. *J. Mater. Sci. Mater. Med.* **1999**, *10*, 697.
(18) Li, D.; Fleet, M. E.; Bancroft, G. M.; Kasrai, M.; Pan, Y. *J. Non-Cryst. Solids* **1995**, *188*, 181.
(19) Peitl, O.; Zanotto, E. D.; Hench, L. L. *J. Non-Cryst. Solids* **2001**, *292*, 115.
(20) Gross, U.; Strunz, V. *J. Biomed. Mater. Res.* **1985**, *19*, 251.
(21) Karlsson, C.; Zanghellini, E.; Swenson, J.; Roling, B.; Bowron, D.T.; Borjesson, L. *Phys. Rev. B* **2005**, *72*, 064206.
(22) Lammert, H.; Heuer, A. *Phys. Rev. B* **2005**, *72*, 214202.
(23) Huang, C.; Cormack, A. N. *J. Chem. Phys.* **1991**, *95*, 3634.
(24) Smith, W.; Greaves, G. N.; Gillan, M. J. *J. Chem. Phys.* **1995**, *103*, 3091.
(25) Vollmayr, K.; Kob, W.; Binder, K. *Phys. Rev. B* **1996**, *54*, 15808.
(26) Horbach, J.; Kob, W.; Binder, K. *J. Phys. Chem. B* **1998**, *103*, 4104.
(27) Cormack, A. N.; Du, J.; Zeitler, T. R. *Phys. Chem. Chem. Phys.* **2002**, *4*, 3193.
(28) Tischendorf, B. C.; Alam, T. M.; Cygan, R. T.; Otaigbe, J. U. *J. Non-Cryst. Solids* **2003**, *316*, 261.
(29) Ganster, P.; Benoit, M.; Kob, W.; Delaye, J. M. *J. Chem. Phys.* **2004**, *120*, 10172.
(30) Linati, G.; Lusvardi, G.; Malavasi, G.; Menabue, L.; Menziani, M. C.; Mustarelli, P.; Segre, U. *J. Phys. Chem. B* **2005**, *109*, 4989.
(31) Du, J; Corrales, R. L. *Phys. Rev. B* **2005**, *72*, 092201.
(32) Car, R.; Parrinello, M. *Phys. Rev. Lett.* **1985**, *55*, 2471.
(33) Tilocca, A.; de Leeuw, N. H. *J. Mater. Chem.* **2006**, *16*, 1950.
(34) Donadio, D.; Bernasconi, M.; Tassone, F. *Phys. Rev. B* **2004**, *70*, 214205.
(35) Charpentier, T.; Ispas, S.; Profeta, M.; Mauri, F.; Pickard, C. J. *J. Phys. Chem. B* **2004**, *108*, 4147.
(36) Smith, W.; Forester, T. R. *J. Mol. Graph.* **1996**, *14*, 136.
(37) Tilocca, A.; de Leeuw, N. H.; Cormack, A. N. *Phys. Rev. B* **2006**, *73*, 104209.

intermediate (BG55) to bioinactive (BG65); the first two are often used in experiments and (in the case of BG45, which corresponds to the original 45S5 Bioglass discovered by Hench) biomedical applications, whereas the latter is a useful nonbioactive reference. The results of these simulations enable us to investigate whether and how the key structural properties discussed above are affected when the silica content increases and the bioactivity decreases.

2. Computational Methods

Force Field. Classical molecular dynamics simulations were carried out with the DL_POLY code[36] using an ionic interatomic potential model recently developed in our group to model silicate glasses incorporating Na and Ca cation modifiers.[37] A shell-model approach[37−39] is used in the potential to effectively include polarization effects, taking into account the large polarizability of oxide ions: the total charge Z of the ion is split between a core (of charge $Z + Y$) and a shell (of charge $-Y$), which are coupled by a harmonic spring. Besides the damped[37] harmonic interaction with the corresponding core, the oxygen shells interact with each other and with Si, Na, Ca, and P cations through a short-range Buckingham term, whereas coulombic forces act between all species, which bear full formal charges. In addition, three-body screened harmonic potentials are used to control the intra-tetrahedral O−Si−O and O−P−O angles. The derivation of the new potential and its implementation in MD simulations is described fully in ref 37; it is worth remarking here that the parameters describing Na−O and Ca−O interactions were fitted to the structures of crystalline silicate phases as identified in typical bioglass and glass−ceramics compositions[19,30,37] and are therefore adequate to model bioactive silicate glasses. In addition to these existing parameters, the P−O pair interaction parameters have been fitted to the structure of α-Na_3PO_4, β-$Ca_3(PO_4)_2$, and $NaCaPO_4$[40−42] by keeping the other interaction parameters fixed. Unlike the silicate case, in which the effective O−Si−O force constant had to be increased with respect to the original value obtained for quartz[43] in order to improve the silicon coordination number for glasses,[37] this adjustment was not needed for the phosphate group: the three-body O−P−O interaction constant (scaled by the screening exponential factor with P−O distances of 1.6 Å) is essentially the same as in previous MD simulations of silicon aluminophosphates.[44]

The complete potential model, together with the lattice constants obtained after energy minimization with the fitted parameters, is reported in the Supporting Information. A small time step is required to control the high frequency of the core−shell spring in the MD simulations: 0.2 fs was used, leading to fluctuations of less than 0.005% and no overall drift in the total energy. Cubic periodic boundary conditions are applied, with a cutoff of 8 Å for the short-range interactions, as well as the Ewald summation of the long-range coulomb interactions.

Glass Generation. The three glass compositions examined contain 45, 55, and 65 wt % SiO_2, a constant low amount (6 wt %) of P_2O_5, and equal percentages (24.5, 19.5, and 14.5 wt %, respectively) of Na_2O and CaO. Table 1 reports the exact composition of our systems and the corresponding molar percentages. The melt-derived glass structures were obtained using a standard molecular dynamics melt-and-quench approach.[37] The appropriate number of ions (around 1500) was randomly inserted in a supercell whose volume was chosen to reproduce the experimental density[12] at room temperature (RT) of 2.702 and 2.655 g cm^{-3} for BG45 and BG55, respectively, whereas for BG65, for which experimental density data are not available, the Doweidar's method[11,45] allowed us to estimate a density of 2.553 g cm^{-3}. The resulting size of the cubic simulation cells is also reported in Table 1. The random initial configuration was heated and held at 3500 K for 60 ps in the NPT ensemble, ensuring a suitable melting of the sample. The liquid was then continuously cooled to 1000 K at a quench rate of 10 K/ps[46] in another constant-pressure run of 250 ps, followed by a constant-volume run of 70 ps in which the system was further cooled to RT with its volume gradually adjusted to the final value, corresponding to the experimental density (without this adjustment, a full NPT quench to RT led to a theoretical density around 5% lower than the experiment). The resulting glass structure was then used in a final NVT trajectory of 200 ps, the last 150 ps of which were included in the structural analysis. In each case, two different glass samples, obtained by starting the melt−quench procedure from different random initial configurations, were generated and their structural properties averaged in order to improve the statistical accuracy for each composition. Test calculations, comparing average structural properties calculated from MD trajectories of different length (up to 1 ns), showed that converged structural properties are already obtained after ∼100−200 ps; although longer trajectories would be needed to investigate dynamical properties such as ion mobilities,[22] this shorter time scale is generally used with good results in MD studies of glass structural properties.[48,49]

Table 1. Details of the Simulated Systems

	SiO_2	Na_2O	CaO	P_2O_5	cell side (Å)
		BG45			
mol %	46.1	24.35	26.90	2.57	26.734
N of species	233	123	136	13	
		BG55			
mol %	56.5	19.40	21.47	2.63	27.371
N of species	300	103	114	14	
		BG65			
mol %	66.9	14.47	15.98	2.63	27.766
N of species	356	77	85	14	

3. Results and Discussion

3.1. Short- and Medium-Range Order. *Silicate and Phosphate Groups.* Three snapshots of the glasses, extracted from the molecular dynamics runs, are shown in Figure 1 The short-range order of the glass structures can be analyzed through the radial distribution functions (rdfs) relative to the

(38) Dick, B. G.; Overhauser, A. W. *Phys. Rev.* **1958**, *112*, 90.
(39) Mitchell, P. J.; Fincham, D. J. *J. Phys. Condens. Matter* **1993**, *5*, 1031.
(40) Harrison, R. J.; Putnis, A.; Kockelmann, W. *Phys. Chem. Chem. Phys.* **2002**, *4*, 3252.
(41) Yashima, M; Sakai, A.; Kamiyama, T.; Hoshikawa, A. *J. Solid State Chem.* **2003**, *175*, 272.
(42) Ben Amara, M; Vlasse, M.; Le Flem, G.; Hagenmuller, P. *Acta Crystallogr., Sect. C* **1983**, *39*, 1483.
(43) Sanders, M. J.; Leslie, M.; Catlow, C. R. A. *J. Chem. Soc., Chem. Commun.* **1984**, 1271.
(44) Sastre, G; Lewis, D. W.; Catlow, C. R. A. *J. Phys. Chem.* **1996**, *100*, 6722.
(45) Doweidar, H. *J. Non-Cryst. Solids* **1999**, *249*, 194.
(46) The short time scale of computer simulations requires a cooling rate γ several orders of magnitude higher than typical experimental rates. This is known to result in a glass transition temperature (T_g) significanly higher than the actual one: indeed, a plot of enthalpy vs temperature[25] allows us to estimate $T_g \approx 1030$ K for BG45, about 220 K higher than the experimental value.[47] However, previous simulations showed that, despite the different T_g, γ around 10 K/ps yields converged and accurate structural properties[25] and is used in most MD studies of melt-derived glasses and bioglasses.[29−31,49]
(47) Andersson, O. H. *J. Mater. Sci. Mater. Med.* **1992**, *3*, 326.
(48) Palin, E. J.; Trachenko, K. O.; Dove, M. T. *J. Phys. Condens. Matter* **2002**, *14*, 4857.
(49) Mead, R.; Mountjoy, G. *J. Phys. Chem. B* **2006**, *110*, 14273.

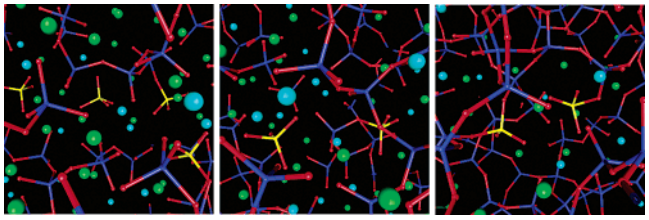

Figure 1. Structure of the simulated glasses: left, BG45; center, BG55; right, BG65. Color codes: red, oxygen; blue, silicon; yellow, phosphorus; dark green, sodium; cyan, calcium; sodium and calcium ions are shown as spheres, whereas silicon, phosphorus, and oxygen are shown as ball-and-stick models.

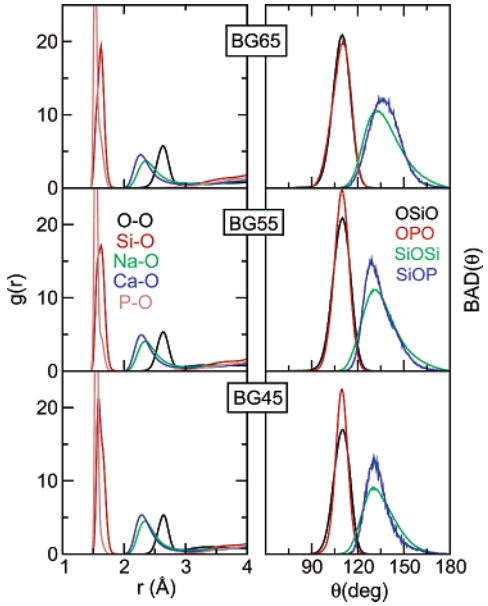

Figure 2. (left panels) Radial distribution functions of oxygen ions; (right panels) bond-angle distribution functions: TOT and OTO (T = Si, P) angles.

Table 2. Selected Average Distances (Å) and Angles (deg)

	BG45	BG55	BG65
r_{Si-O}	1.59	1.62	1.62
r_{P-O}	1.55	1.55	1.53
r_{O-O}	2.64	2.64	2.63
r_{Si-Si}	3.04	3.03	3.02
r_{Na-O}	2.34	2.34	2.35
r_{Ca-O}	2.29	2.29	2.28
r_{Na-Na}	3.25	3.15	3.4
r_{Ca-Na}	3.5	3.5	3.6
r_{Ca-Ca}	3.6	3.65	3.7
$\theta_{Si-O-Si}$	131(24)	131.5(25)	132(28)
θ_{P-O-Si}	131(15)	129(17)	137(22)
θ_{O-Na-O}	60−89	60−89	59−88
θ_{O-Ca-O}	58−84	57−86	55−83

oxygen ions, shown in the left panels of Figure 2, whereas Table 2 reports the relevant average distances, corresponding to the rdf maximum. The general features are essentially unchanged in the three compositions: the intratetrahedral P−O distance of 1.53−1.55 Å, close to the P−O distance of 1.52 Å in $AlPO_4$,[50] is slightly shorter than the Si−O distance of around 1.6 Å, typical of silicate glasses. The shoulder at 1.62 Å in the P−O peak for the BG55 and BG65 compositions comes from P−BO pairs: it becomes increasingly more marked as the percentage of bridging oxygens in the glass increases with the silica content. In our simulations, phosphate groups are found as isolated orthophosphates (Q^0), pyrophosphates Q^1, and metaphosphates Q^2, whose relative fractions change with the glass composition (see section 3.2). According to neutron diffraction data on phosphate glasses,[51] Q^0, Q^1, and Q^2 phosphate groups in these materials should exhibit P−NBO distances between 1.48 and 1.54 Å, and P−BO distances between 1.61 and 1.64 Å, both in agreement with our results. Therefore, the local geometry of phosphate tetrahedra, and in particular the different strengths of P−NBO and P−BO bonds, is correctly reproduced with the present potential model, using the new P−O interaction parameters fitted in this work. The O−T−O bond angle distributions (BADs) in the right panels of Figure 2 centered at the tetrahedral angle show that O−P−O angles tend to be more rigid than O−Si−O. Because this effect disappears with increasing silica content, it is likely related to the different environment of phosphate groups in these glasses: the rigid intratetrahedral arrangement of orthophosphate groups (predominant in BG45) is increasingly perturbed when one or two of the four bonded oxygens form a bridge with a silicon atom, as in BG55 and BG65 (see below). The nearest-neighbor Na−, Ca−, and O−O distances are very close to the values previously obtained for sodium and soda-lime silicate glasses, with higher silica content.[37] In summary, the short-range arrangement of these glasses turns out to be rather rigid and hardly affected by the composition: previous X-ray diffraction (XRD) measurements showed similar patterns for BG45 and BG55, denoting similar structural ordering up to the first-nearest neighbor.[12]

To the best of our knowledge, no experimental data on the intertetrahedral structure have been obtained for bioactive glasses; we previously showed that the inclusion of polarization effects with the present potential is crucial for obtaining an accurate reproduction of the Si−O−Si angle in sodium and soda-lime silicate glasses,[37] and the same likely applies for the bioactive glasses. Structural features beyond the first-nearest neighbor have a higher degree of flexibility and are more affected by the composition than the intratetrahedral structure. The Si−O−Si BAD in Figure 2 (right panels) and the Si−Si first-neighbor distance (Figure 3) reflect the intertetrahedral connectivity: compared to compositions with a higher silica content,[37] the glasses studied here show a shorter Si−Si distance (∼3.03 Å) and, related to it, a smaller Si−O−Si angle, around 132°. This could be a consequence of a higher $(Na_2O + CaO)/SiO_2$ ratio: when the BO of a Si−O−Si linkage also interacts with a cation M, the Si−O−Si angle will decrease to accommodate it. In fact, the $10Na_2O-15CaO-75SiO_2$ glass studied in ref 37, whose Si−O−Si angle is around 140°, has an average BO−M (M = Na + Ca) coordination number of 0.7 (0.5 Na and 0.2 Ca), to be compared with the higher BO−M coordination numbers reported in Table 3 for the glasses studied here: for BG45, each BO is associated, on average, with 1.5 Na atoms and 0.3 Ca ions.

The P−O−Si angle is close to the Si−O−Si one for BG45 and BG55 glasses, whereas it is slightly larger for the BG65 composition. The spread of both T−O−T angle distributions,

(50) Thong, N.; Schwarzenbach, D. *Acta Crystallogr., Sect. A* **1979**, *35*, 658.

(51) Hoppe, U.; Walter, G.; Kranold, R.; Stachel, D. *J. Non-Cryst. Solids* **2000**, *263*−264., 29.

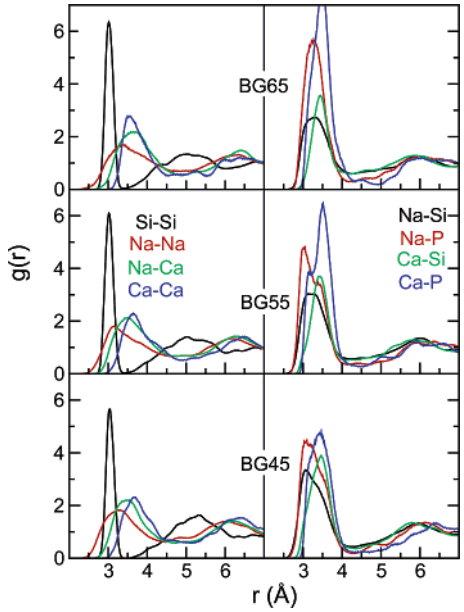

Figure 3. (left panels) Radial distribution functions of X−X (X = Na, Ca, Si) pairs; (right panels) radial distribution functions of Si(P)−Na(Ca) pairs

Table 3. Coordination Numbers: Integral of the Corresponding Radial Distribution Function up to the First Minimum

	BG45	BG55	BG65
CN_{Na-O}	5.8	5.95	5.9
CN_{Ca-O}	6.1	6.1	6.1
CN_{Na-NBO}	4.4	3.8	3.2
CN_{Ca-NBO}	5.5	5.1	4.75
CN_{Na-Na}[a]	5.75 (5.74)	4.4 (4.26)	3.3 (2.76)
CN_{Ca-Ca}[a]	3.2 (2.73)	2.45 (1.91)	1.75 (1.08)
CN_{Na-Ca}	3.3	2.75	1.95
CN_{Si-Na}	5.26	4.1	2.83
CN_{Si-Ca}	2.94	2.10	1.41
CN_{P-Na}	6.24	4.87	4.00
CN_{P-Ca}	3.63	3.36	2.75
CN_{Si-NBO}	1.94	1.22	0.77
CN_{P-NBO}	3.55	3.25	2.74
CN_{BO-Na}	1.5	1.05	0.7
CN_{BO-Ca}	0.3	0.25	0.2

[a] The values between parentheses following CN_{Na-Na} and CN_{Ca-Ca} are the corresponding values estimated for a homogeneous distribution.

as measured by the fwhm reported in parentheses after the corresponding angle in Table 2, generally increases with increasing silica content; P−O−Si linkages appear more rigid than Si−O−Si, judging from the broader Si−O−Si angle distribution, especially for the BG45 composition.

Na−Ca Local Environment. The local coordination environment surrounding modifier sodium and calcium ions can be investigated through the coordination numbers shown in Table 3. These were calculated by integrating the corresponding rdfs up to the distance corresponding to the first minimum. Both Na and Ca ions are enclosed in a pseudooctahedral coordination shell of about six oxygens, as also evidenced by the O−Na(Ca)−O BADs (not shown), featuring two peaks at 60° (arising from BO−M−BO or BO−M−NBO triads) and 90° (NBO−M−NBO triads). As already observed for soda-lime silicate glasses,[33,37,52] calcium has a higher preference for coordination by NBO compared to sodium: for BG45, 90% of the Ca coordination shell is composed of NBOs, considerably more than the 70% total fraction of NBO in this glass, whereas the composition of the sodium coordination shell closely matches the BO:NBO statistical ratio. This preference of Ca for NBOs becomes increasingly more marked in the BG55 and BG65 glasses: although the overall lower fraction of NBOs leads to a decrease in the absolute number of NBOs in the Ca coordination shell, the NBO fraction around Ca is considerably higher (up to two times for BG65) than the total NBO fraction in the glass. It is interesting that sodium also starts to show a preference (although much less marked than Ca) for NBO coordination with increasing silica content.

3.2. Coordination and Network Connectivity. *Silicon.* Table 4 denotes ideal 4-fold coordination for Si in BG45 (Si^4 in the table) and a very small fraction (less than 0.5%) of fivefold-coordinated Si^5 defects in BG55 and BG65. It should be remarked that the three-body O−Si−O interaction parameters had been tuned in such a way to control the occurrence of these defects in modified silicate glasses,[37] and the very low fractions observed here for BG55 and BG65 are in fact reasonable.[56] Although the very small fraction of these defects does not affect the structural properties examined in this work, they might play an important role when dynamical and reactive properties are considered.

In silicate glasses, the addition of network-modifier M ions (Na and Ca) disrupts the three-dimensional silicate network by breaking Si−BO−Si bridges, which are replaced by Si−NBO−M units. Therefore, the Q^n distribution of modified silicate glasses is shifted toward low n values, compared to high-silica compositions that are predominantly Q^4. We have previously shown[37] that, compared to rigid-ion potentials, the shell model leads to a more reliable Q^n distribution for modified silicate glasses. Table 4 shows that silicon in BG45 is predominantly Q^2, whereas Q^3 is the most common Si species in BG55 and BG65 glasses. This general trend qualitatively follows experimental NMR findings on similar and related compositions;[11] moreover, recent Raman data on BG45 and BG55[12] yield Q^2 and Q^3 abundancies close to our corresponding estimates (Table 4). The existence of more than two different Q^n species for these glasses is the subject of active debate; a source of uncertainty is the intrinsic difficulty in detecting species such as Q^1 and Q^4 present at low concentration, whose signal partially overlaps with the signal of the predominating Q^n sites. Although a binary model (with only Q^2 and Q^3 present) is sometimes assumed,[9,11] other experimental data have been interpreted with up to four Q^n (from Q^1 to Q^4) species simultaneously present.[10,12,53] Our calculated Q^n distributions denote the presence of 3−4 Q^n species in the three compositions, with significant amounts of Q^1 for BG45 and Q^4 for BG55 and BG65. It is interesting to note that we detect a small amount of orthosilicate (Q^0) species in the BG45 glass only, in agreement with the findings of ref. 12. Because the migration and release of isolated orthosilicate groups into solution are

(52) Cormack, A. N.; Du, J. *J. Non-Cryst. Solids* **2001**, *293*, 283.
(53) Schneider, J.; Mastelaro, V. R.; Zanotto, E. D.; Shakhmatkin, B. A.; Vedishcheva, N. M.; Wright, A. C.; Panepucci, H. *J. Non-Cryst. Solids* **2003**, *325*, 164.
(54) Kim, Y. S.; Tressler, R. E. *J. Mater. Sci.* **1994**, *29*, 2531.
(55) Zeitler, T. R.; Cormack, A. N. *J. Cryst. Growth* **2006**, *294*, 96.
(56) Stebbins, J. F.; McMillan, P. *J. Non-Cryst. Solids* **1993**, *160*, 116.

Table 4. Coordination and Network Connectivity[a]

	Q^n (Si)						Q^n (P)			O coordination			Si coordination		
	Q^0	Q^1	Q^2	Q^3	Q^4	Q^5	Q^0	Q^1	Q^2	O^0	O^1	O^2	Si^4	Si^5	NC
BG45	1 (10)	20 (8)	53 (58)	24 (24)	2	0	65	33	2	0	68.8	31.2	100	0	2.07
BG55	0	3 (4)	31 (40)	53 (56)	13	0	34	59	7	0.1	52	48	99.7	0.3	2.77
BG65	0	0	9	58	32	1	9	56	35	0	37.2	62.8	99.7	0.3	3.24

[a] The values in parentheses are the experimental Q^n(Si) abundancies (±5%) estimated by Raman spectroscopy.[12]

faster than those of Q^n species with $n > 1$, the presence of these species only in BG45 could be a key factor in its higher bioactivity. On a similar basis, BG45 also has a greater fraction of Q^1 silicates, and a corresponding lower fraction of less mobile Q^3 and Q^4 species.

The average number of NBO per Si atom (CN_{Si-NBO} in Table 3) sharply decreases from almost 2 for BG45 to 0.77 for BG65, reflecting a considerable change in the arrangement of the silicate network, which becomes much less fragmented; the number of NBO per P atom also decreases, although not as sharply as for the silicates, from NBO/P = 3.55 for BG45 (NBO/P = 4 would correspond to a pure orthophosphate) to NBO/P = 2.74 for BG65. The network connectivity of the simulated glasses (Table 4), calculated from the Q^n distribution, is analogous to the Stevel's *Y* parameter, which describes the average number of BO per tetrahedron.[14] On the basis of specific assumptions on the coordination environments of Si and P, researchers predicted a critical value of 1.9 for the NC of BG45.[16] Our simulations allow us to directly measure NC without any a priori assumption, as the correct fraction of Si−O−P links and the possible occurrence of coordination defects are taken into account. Table 4 shows that BG45 has NC = 2.07, slightly larger than the theoretical value; the network connectivity increases with the silica content, up to 3.24 for the nonbioactive BG65.

Phosphorus. It is normally assumed that phosphate groups are predominantly isolated orthophosphates (associated with modifier M ions) in BG45 and similar compositions with a low amount of P_2O_5, and NMR and Raman measurements support this view.[11,12,57] The lower strength of P−O−Si than of Si−O−Si bonds and the greater stability of P−O−M than of Si−O−M bonds may explain this observation,[57] together with the low P_2O_5 concentration and the local charge imbalance of Si−O−P substitution, for instance, compared to more favorable Al−O−P bridges in aluminophosphates. However, although the above factors do not allow a full incorporation of P as a network former in the glass, it is not clear up to what extent the phosphate groups are completely separated from the silicate network: the occurrence of P−O−Si bridges involving one of the four bonded oxygen atoms in a fraction of the PO_4 tetrahedra would not significantly perturb the overall network arrangement. On the one hand, only Q^0 (P) are reported in some NMR studies;[9,11] on the other hand, cross-linking between silicate and phosphate groups has sometimes been proposed to interpret IR, Raman, and other NMR data,[10,12,18] although the occurrence of Si−O−P links at very low phosphate levels is not clear-cut. The identification of silico-phosphate crystalline phases with Si−O−P linkages after crystallization of the corresponding gel glasses also shows that these links can be stable in the glassy state.[54] Recent MD simulations of bioactive silicate glasses using rigid-ion potentials,[30,55] pointed to the coexistence of Q^0 and Q^1 phosphates, the latter being involved in a small but still relevant number of Si−O−P links. As in the case of the Si Q^n coordination, these discrepancies are probably related to the uncertainties in the NMR or Raman spectral signatures of a Q^0 (P) and a Q^1 (P), or in deconvoluting the signal of Si−O−Si and Si−O−P links, especially when the latter are present at a much lower concentration. Our simulations show that orthophosphate species are indeed predominant for BG45, but a fraction of phosphate groups are linked to a single (Q^1 (P) species) or two (Q^2 (P)) Si atoms. The large majority (95%) of Si ions is not linked to phosphorus. The relative fraction of Q^1 (P) and Q^2 (P) sites increases with increasing silica content in BG55 and BG65; the increasing tendency of phosphorus to form cross-links in the BG45−BG55−BG65 series, which contain the same phosphate molar fraction, is related both to the higher percentage of SiO_2 and to the lower availability of Na and Ca cations to neutralize the orthophosphate groups. Because the phosphate potential was fitted to the structure of crystalline orthophosphates, with no Si−O−P links, their formation in the silicate glasses studied here was not biased by the parametrization procedure. The formation of P−O−P cross-links is statistically less likely than P−O−Si, because of the low P_2O_5 concentration; it is interesting that, although no P−O−P links are present for BG45 and BG55, the only case in which they are formed in our MD simulations is the bioinactive BG65, which is characterized by the occurrence of phosphate-rich regions (see below).

3.3. Ion Aggregation. *Phosphate and Silicate Domains.* A first insight into the microenvironment around phosphate and silicate groups comes from the rdfs of Na/Ca−Si/P pairs, shown in the right panels of Figure 3. Fairly sharp first-neighbor peaks are present for all pairs, indicating formation of Na and Ca shells with a well-defined radius of 4.5 Å around the silicate and phosphate tetrahedra. For BG45, Table 3 shows that about eight modifier cations are found on average in the shell surrounding SiO_4, whereas a larger number of cations (∼10) are found around PO_4 groups. The general preference of modifier cations for phosphate groups confirms their general repolymerizing effect on the silicate network,[9,57] observed for silicate melts and bioglasses. Although the total number of cations in both Si and P shells significantly decreases in going to BG65, the preference for PO_4 becomes increasingly more marked, leading to the formation of cation-rich regions around PO_4, such as those shown in Figure 5 for BG65.

The structural arrangement of the Na/Ca shells surrounding Si and P centers is described by the distribution of M−T−M

(57) Mysen, B. O.; Ryerson, F. J.; Virgo, D. *Am. Mineral.* **1981**, *66*, 106.

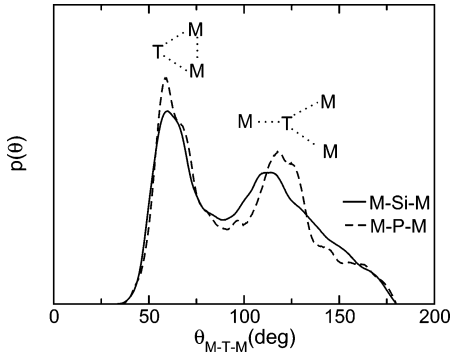

Figure 4. Distribution of M−T−M (M = Na/Ca, T = Si/P) angles for the BG45 composition. No significant differences are found for BG55 and BG65. The polygonal structures corresponding to the two peaks are sketched.

Table 5. $R^{A}_{B/C}$ Ratios

	BG45	BG55	BG65
$R^{Si}_{Na/Ca}$	1.00	1.08	1.11
$R^{P}_{Na/Ca}$	0.96	0.80	0.80
$R^{Si}_{Si/P}$	1.01	1.07	1.15
$R^{P}_{Si/P}$	0.74	0.73	0.76

(M = Na/Ca, T = Si/P) angles shown in Figure 4, where the two most common structural arrangements are also sketched: the main peak at about 60° denotes closed, roughly equilateral triangles with the vertices occupied by two modifier cations and a Si(P) atom: the typical M−T and M−M distances are indeed in the same range. A secondary peak located around 120° arises from M−M−M triads with a Si or P ion in the center.

The rdfs in the right panels of Figure 3 denote an increasingly significant Ca−P interaction with increasing silica content. To investigate this point, we can use the calculated coordination numbers of B ions around a central A ion, CN_{A-B}, provided that the different total number of A and B ions in each composition is taken into account by an adequate weighting. To this purpose, we define the ratio $R^{A}_{B/C} = CN_{A-B}/CN_{A-C}$ and normalize it with respect to the number ratio N_B/N_C of ions B and C in the cell. A unit ratio will then denote a statistical (random) distribution of B and C ions surrounding A, strictly following their different concentration, whereas deviations from unity denote a non-statistical environment around the central ion A: a ratio greater than 1 denotes preference of A for coordination of B ions, whereas a ratio lower than 1 denotes preference of A for coordination of C ions. Table 5 shows that for BG45 both modifier cations are randomly distributed around Si and P centers; however, with decreasing bioactivity, there is an increasing preference of Na for silicate, and especially of Ca for phosphate groups. The same approach also allows us to measure the level of aggregation between SiO_4 and PO_4 groups: the $R^{P}_{Si/P}$ ratio in Table 5 shows a marked preference of phosphate groups to be located close to another phosphate, rather than to a silicate. This denotes a clear tendency of phosphate groups to aggregate with each other for the three compositions studied here; this interaction mainly involves orthophosphate groups. These PO_4-rich regions generally involve a small number of phosphates, around 4−5, as shown in Figure 5; their size probably increases in similar silicate glass structures with higher

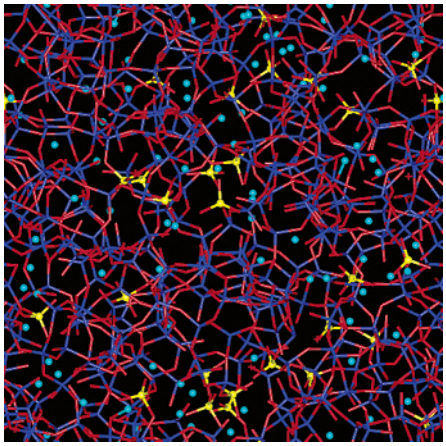

Figure 5. Phosphate-rich regions in the BG65 structure. Color codes are the same as Figure 1; for clarity, only Ca modifier ions are shown here.

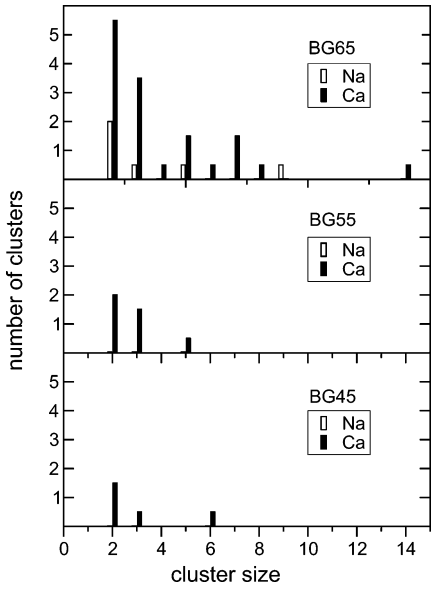

Figure 6. Distribution of the size of clusters formed by sodium and calcium ions in the three compositions studied.

phosphate content. The enhanced self-aggregation of phosphates also leads to a lower concentration of phosphate groups around Si than expected on a statistical basis; together with the higher silica content going from BG45 to BG65, this leads to the corresponding increasing trend of the $R^{Si}_{Si/P}$ ratio.

Clustering of Modifier Cations. Although the cation−cation rdfs in the left panels of Figure 3 show some structuring, it is not straightforward to infer from them whether the cations show a significant tendency to aggregate with each other. Therefore, we directly investigated the formation of clusters of Na/Ca ions using a simple, effective rule:[49] each pair of ions coordinated to the same oxygen was considered as part of the same cluster, and the distribution of cluster sizes was determined for the three glass compositions following this rule. The distributions in Figure 6 shows that sodium is uniformly distributed in the cell and does not form clusters in BG45 and BG55, whereas a few small sodium clusters, well-separated from the remaining ions, are identified in BG65.[58] A rather homogeneous distribution, with the formation of only a few small clusters, is also observed for Ca ions in BG45 and BG55; however, a

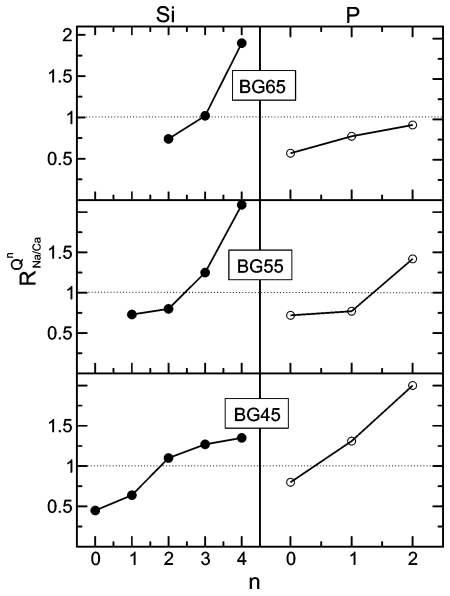

Figure 7. $R^{Q^n}_{Na/Ca}$ ratios for Si (left) and P (right) Q^n centers. $R > 1$ denotes preference of Q^n for Na coordination, whereas $R < 1$ indicates Ca preference.

markedly different behavior of Ca in BG65 emerges, with Ca ions arranged in clusters whose size ranges between 2 and 15 atoms. Similar conclusions are reached if the M−M coordination numbers for Na and Ca are compared with those expected for a homogeneous distribution of ions, given by $CN^{hom}_{M-M} = (4/3)\pi R_c^3 \rho(M) - 1$, where R_c is the cutoff distance corresponding to the first rdf minimum and $\rho(M)$ is the number density of M cations in our systems.[49] The CN^{hom}_{Na-Na} and CN^{hom}_{Ca-Ca} values calculated for the three glass compositions are reported following the corresponding MD values in Table 3: as the silica content increases, Ca−Ca coordination numbers become increasingly larger than the corresponding CN^{hom}_{Ca-Ca}, and large deviations are observed for BG65; on the other hand, the calculated CN_{Na-Na} are close to a uniform distribution for BG45 and BG55 and show a moderate tendency to cluster only for BG65.

Q^n Modifier Interaction and Glass Solubility. As the Na_2O:CaO proportion is increased with respect to typical bioactive compositions, one obtains very soluble glasses, which are completely resorbed a short time after implant.[1] An interpretation of this effect involves the high solubility of sodium silicates with sodium linked to low-*n* Q^n sites such as Q^2: when Ca ions are also present, they displace sodium from these sites, forming less-soluble microphases.[9] We can determine the coordination of Na and Ca around the different Q^n units by decomposing the Na(Ca)−Si(P) rdfs into the contributions of the Na(Ca)−Q^n pairs. As before, we normalize the number of Na and Ca coordinated to each Q^n by the Na/Ca number ratio in the cell, so that $R^{Q^n}_{Na/Ca} > 1$ denotes preference of the Q^n species for Na, whereas $R^{Q^n}_{Na/Ca} < 1$ denote preference for Ca. Figure 7 (left column) shows a net preference of Ca for low-*n* Q silicate sites that is much stronger than that of Na ions, which are then displaced toward high-*n* sites. This is clearly reflected in the higher percentage of NBO in the Ca coordination shell, discussed before. For the more soluble BG45, sodium predominates around Q^n species with $n \geq 2$, whereas Ca displaces Na away from the Q^1 species; for BG55 and BG65, Ca gradually displaces Na from Q^2 and Q^3 species as well. A similar trend is observed for phosphorus: Figure 7 (right column) shows that Q^0 (P) phosphates are always mostly associated with Ca. For BG65, Ca displaces Na out of all the Q^n (P) species, confirming Ca/P aggregation at this composition, whereas for BG45, Na dominates the coordination of pyrophosphate Q^1 and metaphosphate Q^2 sites; BG55 is intermediate between BG45 and BG65. These data therefore support the existence of a strong link between glass solubility and local cationic microenvironment of silicate and phosphate groups.

3.4. Discussion. Putting together the main findings above, a structural model of of silicate glasses emerges that links the bioactive behavior to the combined effects of the connectivity of the extended silicate network and to the tendency to form (or not to form) nonuniform domains. According to the calculated network connectivities, taking into account that BG55 is still bioactive, whereas BG65 is not, we can propose an upper NC limit of around 3 for bioactivity: compositions with network connectivity higher than 3 should not be bioactive. The BG45 NC of ∼2 denotes a fragmented, open structure, with silicate Q^2 as the main feature; direct inspection of the structures reveals some Q^2 chains containing up to eight units. These relatively long Q^2 chains, not present for the two other compositions, could then be involved in the high bioactivity of BG45, because they can be directly released into solution without breaking any Si−O bonds in step (b) of the bioactive mechanism.[16] A NC exceeding 3 denotes that most silicate units are significantly cross-linked to each other, forming a three-dimensional network dominated by Q^3 and Q^4 units; because the release of soluble silica fragments now requires breaking several Si−O bonds, this dissolution process is much less favored and its slower rate is probably a main factor determining bioinactivity. The aggregation of (ortho)phosphates and the preference of modifier cations for phosphate is common to all three compositions, leading to cation-rich domains that contain a significantly larger amount of phosphate than a random distribution; for BG45, these regions are randomly populated with Na and Ca cations, whereas loss of bioactivity by going to BG55 and BG65 is accompanied by increasing Ca/P and Na/Si aggregation. In other words, moving away from the bioactivity range, we see a tendency toward the formation of Ca-rich phosphate and Ca-poor silicate regions. The formation of amorphous phase-separated regions within the glass matrix and the consequent immobilizations of soluble ions has been reported to increase the dissolution resistance for multicomponent silicate glasses;[59] our data suggest that this effect could be an additional reason of the bioinactivity of BG65 and similar compositions. It could be argued that the fast cooling rate may hinder Na ions from finding a thermodynamically more stable and inhomogeneous distribution during glass formation; however, in our opinion, this possibility is ruled out

(58) For BG45 and BG55 compositions, the cluster search algorithm actually detects a single, large sodium "cluster" that involves all the Na ions: in other words, for these glasses, Na ions are homogeneously spread over the simulation cell and do not form small, isolated clusters whose size is in the range plotted in Figure 6.

(59) We, H. F.; Lin, C. C.; Shen, P. *J. Non-Cryst. Solids* **1997**, *209*, 76.

by the reliability of the intermediate-range structure and connectivity calculated for the present MD-quenched models, which entails an equally good representation of other structural properties.

4. Conclusions

The accuracy of the present simulations, on the basis of a reliable treatment of polarization effects, allows us to draw a new microscopic picture of bioactive silicate glasses with different silica content. In agreement with experimental data, we find that phosphate groups are predominantly isolated as orthophosphate units and that the silicate network is dominated by Q^2 and Q^3 sites. However, our simulations show an increasing tendency of phosphate to cross-link to the silicate network with increasing silica content and support the existence of up to four silica Q^n species in the same glass, showing that a simple binary model may be inadequate to describe the network of these materials. On the basis of an accurate explicit calculation of the network connectivity, we estimate an upper limit of three for the network connectivity of bioactive silicate glasses. The three compositions share a tendency to form regions with a high density of phosphate groups, which tend to attract modifier cations in their coordination shell, leading to the formation of cation-rich orthophosphate domains somewhat separated from the cation-poor silicate chains. For the bioactive compositions, these phosphate domains show a uniform mixing of sodium and calcium cations, whereas loss of bioactivity with increasing silica content is accompanied by a net preference for calcium. Therefore, a tendency toward the separation between calcium phosphate and sodium silicate domains seems to emerge as a marker of nonbioactive behavior, confirmed by the enhanced clustering of Ca ions observed only in the bioinactive BG65 glass. In other words, the formation of inhomogeneous regions seems to inhibit the bioactive response of these glasses; a possible explanation is that when phosphate groups associate with each other in these local domains, their mobility is reduced, which slows down their release to the solution, compared to bioactive compositions in which isolated phosphates are embedded in a uniform environment. Further investigations are needed to confirm the reasons of this inhibition effect. Another important future development involves the investigation of the migration rate and mechanism of Na and Ca cations; although this kind of study would require much longer simulation times and/or special simulation techniques to enhance the sampling of the diffusive process, the dynamical properties obtained would be the ideal complement to the structural picture drawn in the present paper.

Acknowledgment. We thank EPSRC for financial support (Grant GR/S77714/01) and for access to the HPCx system via the Materials Chemistry Consortium. The UK's Royal Society is also acknowledged for a University Research Fellowship (A.T.). Additional computing resources were provided by the MOTT2 facility (EPSRC Grant GR/S84415/01) run by CCLRC.

Supporting Information Available: Tables with the interatomic potential form and parameters and with the optimized lattice constants of α-Na_3PO_4, β-$Ca_3(PO_4)_2$, and $NaCaPO_4$. This material is available free of charge via the Internet at http://pubs.acs.org.

CM061631G